

Inelastic scattering of 162-MeV pions by  $^{14}\text{N}$ 

D. F. Geesaman, D. Kurath, G. C. Morrison,\* C. Olmer,<sup>†</sup> and B. Zeidman  
*Argonne National Laboratory, Argonne, Illinois 60439*

R. E. Anderson,<sup>‡</sup> R. L. Boudrie, and H. A. Thiessen  
*Los Alamos National Laboratory, Los Alamos, New Mexico 87545*

G. S. Blanpied<sup>§</sup> and G. R. Burleson  
*New Mexico State University, Las Cruces, New Mexico 88003*

R. E. Segel  
*Northwestern University, Evanston, Illinois 60201*

L. W. Swenson  
*Oregon State University, Corvallis, Oregon 97331*  
 (Received 8 October 1982)

The inelastic scattering of 162-MeV pions by  $^{14}\text{N}$  has been studied over the angular range  $35^\circ$  to  $115^\circ$  in the laboratory system. The data were analyzed with a model which incorporates shell model wave functions into a distorted wave impulse approximation. Reduced transition probabilities obtained for a number of low-lying states are compared to previous data to validate the model. Among new assignments and shell model descriptions presented for several higher excited states is an assignment for the yrast  $5^-$  state.

[ NUCLEAR REACTIONS  $^{14}\text{N}(\pi, \pi')$   $E_\pi=162$  MeV, measured  $\sigma(\theta)$ , ]  
 melamine target, DWIA analysis.

## I. INTRODUCTION

High resolution studies of pion inelastic scattering are relatively recent, and even in the most favorable cases, the reaction mechanism is not completely understood. The present investigation of pion inelastic scattering by  $^{14}\text{N}$  at  $T_\pi=162$  MeV has two purposes. Initially, the extensive nuclear structure information that is available<sup>1</sup> for the low-lying states of  $^{14}\text{N}$  is used to evaluate the reaction model. After this primary step, the properties of the pion-nucleus interaction are used to infer new nuclear structure information.

The approach used is that developed by Lee and Kurath<sup>2</sup> to treat pion inelastic scattering by  $1p$ -shell nuclei. It incorporates well tested wave functions<sup>3,4</sup> into a framework of a distorted wave impulse approximation formulated in momentum space. In the case of  $^{14}\text{N}$ , the states below  $\sim 8.5$  MeV excitation have a relatively simple description that involves  $(1p)^n$  configurations and  $(2s, 1d)^1(1p)^{n-1}$  particle-hole excitations. Comparison of the theoretical predictions with experiment allows validation of the model. The model may then be used as a basis for

interpreting the structure of the higher-lying states of  $^{14}\text{N}$  excited in pion inelastic scattering. In particular, particle-hole configurations of the form

$$[(1d_{5/2})^1(1p_{3/2})^{-1}]_{4-}$$

have been observed<sup>5,6</sup> in pion scattering on the neighboring nuclei  $^{12}\text{C}$  and  $^{16}\text{O}$  at excitation energies of  $\sim 17$  MeV and similar transitions are expected in  $^{14}\text{N}$ . However, the structure in  $^{14}\text{N}$  is more complicated because the  $J^\pi=1^+$  of the ground state allows recoupling and fragmentation of the strength into states with  $J^\pi=3^-, 4^-,$  and  $5^-$ .

Most published data for inelastic scattering to states in  $^{14}\text{N}$  pertain to states with excitation energies  $\leq 13$  MeV although recent  $(\alpha, \alpha')$  and  $(e, e')$  studies<sup>7,8</sup> extend up to  $\sim 16$  MeV excitation. Information on states of higher energies has mainly come from resonances observed in reactions at low energies in which  $^{14}\text{N}$  is the compound nucleus.<sup>9</sup> In particular, states with  $J^\pi=3^-, 4^-,$  and  $5^-$  have been identified, although no configuration information has been obtained. In the  $^{12}\text{C}(d, \alpha)^{10}\text{B}$  reaction, the observation of transitions to the  $T=1$  second excited

state of  $^{10}\text{B}$  for the resonances corresponding to  $^{14}\text{N}$  energies between 16.8 and 22.5 MeV was taken as evidence of isospin mixing in this region. Isospin mixing has also been observed<sup>5,6</sup> in pion inelastic scattering to the  $4^-$  states in  $^{12}\text{C}$  and  $^{16}\text{O}$  and some indication of isospin mixing in  $^{14}\text{N}$  from the present experiment is presented. In the region of interest in  $^{14}\text{N}$ , however, the comparatively large intrinsic widths of the observed resonances ( $\sim 100$  keV) and the high level density present a formidable problem in establishing a correspondence between these previous results and the states observed in the current work. As a consequence, the assignments of spin and parity to the states in  $^{14}\text{N}$  at high excitation energies are primarily inferred from the predictions of pion inelastic scattering using the theoretical structure calculations.

## II. EXPERIMENTAL PROCEDURE

The experiment was performed on the energetic pion channel and spectrometer (EPICS) at the Clinton P. Anderson Meson Physics Facility (LAMPF). The EPICS system<sup>10</sup> has been described previously. The mean energy of the incident  $\pi^+$  or  $\pi^-$  beam was 162.2 MeV, which corresponds to an average energy of 162.0 MeV in the center of the target at forward angles. Positive pion spectra were accumulated at scattering angles from  $35^\circ$  to  $115^\circ$  in  $5^\circ$  steps (no data were taken at  $110^\circ$ ) and negative pion spectra were accumulated at  $35^\circ$ ,  $55^\circ$ ,  $75^\circ$ , and  $95^\circ$ . Short  $\pi^-$  runs were also taken in  $5^\circ$  steps from  $30^\circ$  to  $70^\circ$  in order to measure elastic scattering cross sections. The angular acceptance of the spectrometer was  $\pm 1.5^\circ$ .

The  $^{14}\text{N}$  target used in the experiment was a pressed melamine ( $\text{C}_3\text{H}_6\text{N}_6$ ) plate,  $170$  mg/cm<sup>2</sup> thick; a polyethylene ( $\text{CH}_2$ ) target,  $145$  mg/cm<sup>2</sup> thick was run at each angle to provide reference background spectra. A typical energy spectrum for  $\pi^+$  scattering from each of these targets is shown in Fig. 1, together with a subtracted spectrum corresponding to  $\pi^+$  scattering from  $^{14}\text{N}$ . As is seen in Fig. 1, scattering from carbon produces several strong peaks, corresponding to the collective states in  $^{12}\text{C}$ , and a weaker continuum at higher excitation energies. Because of the large kinematic shift, scattering from hydrogen results in a broad, strong peak whose position changes rapidly in the spectra as the scattering angle is varied. At  $75^\circ$ , only the high energy tail of this peak can be seen in the figure.

The  $\text{CH}_2$  spectra, suitably normalized, shifted, and smoothed to match the resolution of the melamine spectra, were subtracted from the melamine spectra on a channel by channel basis. This pro-

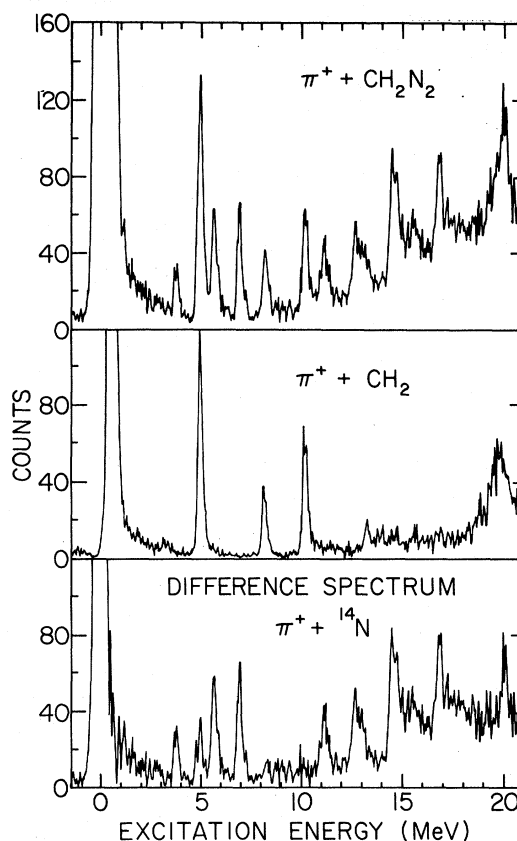


FIG. 1. Spectra for 162-MeV pion scattering at  $75^\circ$  laboratory. The normalized spectra in the upper two sections were subtracted, channel by channel, to yield the  $^{14}\text{N}$  spectrum.

cedure provided clean  $^{14}\text{N}$  spectra except in the immediate vicinity of strong peaks, where statistical errors could result in sizable fluctuations in the yields for adjacent channels, e.g., at excitation energies below 2 MeV in Fig. 1. The peak fitting routine AUTOFIT (Ref. 11) was used to locate centroids of closely spaced levels and to obtain yields. The overall resolution for known discrete states was  $\sim 280$  keV (FWHM) but appears slightly larger at high excitation energies, perhaps reflecting large intrinsic widths for the states.

The relative pion flux for each spectrum was measured in an ionization chamber located downstream of the target. The absolute normalization was determined relative to the known  $\pi^\pm + ^{12}\text{C}$  elastic cross sections<sup>12</sup> at 162 MeV and the stoichiometric composition of the melamine target. The scattering from hydrogen provided an additional normalization, using the known  $\pi + \text{H}$  cross sections,<sup>13</sup> which proved to be consistent with the carbon normaliza-

tion. The relative uncertainty in the differential cross sections resulting from the flux determination is  $\pm 5\%$  (in addition to statistical errors); the absolute cross sections are determined to  $\pm 10\%$ .

### III. EXPERIMENTAL RESULTS

Angular distributions for the elastic scattering of 162-MeV  $\pi^+$  and  $\pi^-$  by  $^{14}\text{N}$  are displayed in Fig. 2. The pronounced oscillations observed in the data are typical of elastic pion scattering in the region of the (3,3) resonance. The frequency of oscillations and positions of minima for  $\pi^+$  and  $\pi^-$  scattering are nearly identical, as is expected for pion scattering by light nuclei.

The spectra of inelastically scattered pions shown in Fig. 1 shows prominent peaks up to an excitation energy of around 20 MeV. At energies less than 13 MeV these peaks correspond to the excitation of individual states in  $^{14}\text{N}$  which are also strongly excited in inelastic scattering of other projectiles.<sup>1</sup> At higher excitation energies, further structure is observed, but the experimental resolution is not good enough to allow positive correlation of these peaks with known states in  $^{14}\text{N}$  or even to be confident that each peak represents a single excited state. Nevertheless, despite the marked increase in the  $^{14}\text{N}$  level density above 12 MeV, it is noteworthy that distinct peaks continue to be observed. Table I lists the excitation energies of states corresponding to the peaks observed and, where possible, their identification with known states in  $^{14}\text{N}$ .

The determination of inelastic yields are subject to

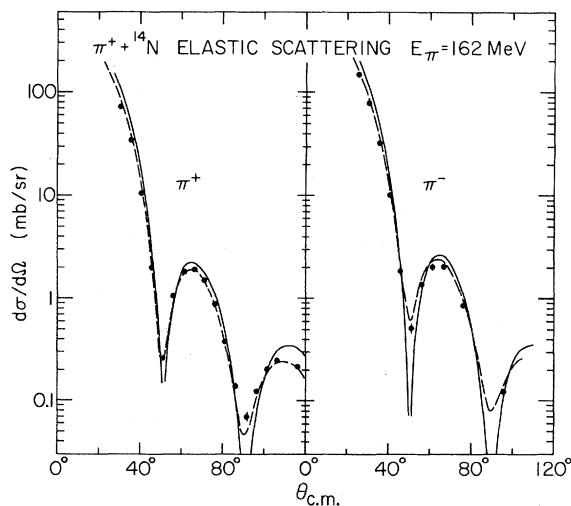


FIG. 2. Elastic scattering of 162-MeV pions by  $^{14}\text{N}$ . The curves are described in the text. The parameters used in the FITPI calculation are the following:  $b_0 = (1.2 - i0.4)$  fm<sup>3</sup>;  $b_1 = (9.8 + i6.7)$  fm<sup>3</sup>;  $R = 1.95$  fm;  $a = 0.44$  fm.

significant errors which arise mainly because of uncertainties in the background due to: (1) the intense C and H elastic and inelastic peaks subtracted out to obtain the  $^{14}\text{N}$  spectra; (2) the intense tail of the  $^{14}\text{N}$  elastic peak, especially at forward angles; (3) the possible presence of weakly-excited unresolved states, especially at forward angles where all  $L$  values contribute; (4) the possible presence of muon events which are not completely rejected. As a result, inelastic data points, particularly for transitions to highly excited states, may be subject to uncertainties in the relative yield additional to the statistical errors and independent of the overall uncertainty in absolute normalization. The uncertainty in the  $\text{CH}_2$  subtraction, however, does not make a major contribution to the error in determining the peak yields, except for the 4.92 MeV state. Angular distributions for the inelastic scattering of  $\pi^+$  and  $\pi^-$  by  $^{14}\text{N}$  are presented in Figs. 3–7; the results will be discussed in the following sections.

### IV. DISCUSSION

In two recent papers, Lee and Kurath<sup>2</sup> developed a method for analysis of inelastic pion scattering at pion energies near the (3,3) resonance which utilizes a first-order distorted wave impulse approximation (DWIA) in momentum space. Within this DWIA framework, they have calculated the excitation of states in  $^{14}\text{N}$  with positive parity that arise from  $(1p)^n$  configurations and also transitions to states of negative parity that result from particle-hole excitations of the form  $(2s,1d)^1(1p)^{n-1}$ . These calculations involve use of the Cohen-Kurath wave functions<sup>3</sup> for  $(1p)^n$  configurations and slightly modified Millener-Kurath wave functions<sup>4</sup> for negative parity states. For the states under discussion, the results are most clearly interpreted in terms of an  $LS$  representation of the relevant particle-hole operators, where  $J$ ,  $L$ , and  $S$  are the total angular momentum, orbital angular momentum, and spin of the particle-hole, pair, respectively. This has the advantage that each  $J$  ( $LS$ ) term exhibits a distinctive angular distribution which may then be weighted by the appropriate  $LS$  amplitude (particle-hole amplitude) for each state to give the calculated angular distribution. Although more than one amplitude may contribute to a given transition, most strong transitions are dominated by a single amplitude which leads to a distinctive angular distribution.

The transition amplitudes in DWIA are expressed in terms of two primary constituents, namely the nuclear transition densities derived from the shell model calculations and the pion-nucleus distorted waves which are derived from analyses of elastic scattering. In the current analysis the nuclear tran-

TABLE I. Summary of results from present study. Levels are listed by excitation energy. Previously assigned spins and parities are underlined. When possible, correspondence to the theoretical predictions of Fig. 8 are indicated under the ID heading. The column labeled "Norm" indicates the ratio of the observed cross section to the theoretical prediction with no enhancement. Where no clear correspondence is possible, Norm also indicates the predicted angular distribution used in Figs. 6 and 7.

$E_x$ (MeV)	$J^\pi$	$T$	ID ( $J^\pi, T$ )	Multipole	Norm
3.95	<u>1<sup>+</sup></u>	0	(1 <sup>+</sup> ,0) <sub>2</sub>	$E2$	1.45±0.2
7.03	<u>2<sup>+</sup></u>	0	(2 <sup>+</sup> ,0) <sub>1</sub>	$E2$	2.2±0.3
4.92	<u>0<sup>-</sup></u>	0	(0 <sup>-</sup> ,0) <sub>1</sub>		10
5.11	<u>2<sup>-</sup></u>	0	(2 <sup>-</sup> ,0) <sub>1</sub>	$E3$	1.15±0.15
5.59	<u>1<sup>-</sup></u>	0	(1 <sup>-</sup> ,0) <sub>1</sub>		10
5.83	<u>3<sup>-</sup></u>	0	(3 <sup>-</sup> ,0) <sub>1</sub>	$E3$	1.54±0.25
8.49	<u>4<sup>-</sup></u>	0	(4 <sup>-</sup> ,0) <sub>1</sub>	$M4 + E3$	1.0(4 <sup>-</sup> ,0) <sub>1</sub> + 0.04(4 <sup>-</sup> ,0) <sub>2</sub>
11.24	<u>3<sup>-</sup></u>	0	(3 <sup>-</sup> ,0) <sub>4</sub>	$E3$	1.9±0.2
12.79	<u>4<sup>-</sup></u>	0	(4 <sup>-</sup> ,0) <sub>2</sub>	$E3$	1.8±0.2
13.14	( <u>2<sup>-</sup></u> )	0		$E3$	0.75±0.2(3 <sup>-</sup> ,0) <sub>4</sub>
14.66	5 <sup>-</sup>	0 + 1	(5 <sup>-</sup> ,0) <sub>1</sub>	$M4$	$\pi^+, 0.75 \pm 0.2 / \pi^-, 0.5 \pm 0.1$
15.1				( $E3, M4$ )	
15.56	2,3,4 <sup>-</sup>	0		$E3$	1.2(3 <sup>-</sup> ,0) <sub>4</sub>
16.06	3 <sup>-</sup>	0	(3 <sup>-</sup> ,0) <sub>8</sub>	$M2$	1.0 + 0.25
16.86	5 <sup>-</sup>	1 + 0	(5 <sup>-</sup> ,1) <sub>2</sub>	$M4$	$\pi^+, 1.1 \pm 0.15 / \pi^-, 0.7 \pm 0.2$
17.46	5 <sup>-</sup>	0 + 1	(5 <sup>-</sup> ,0) <sub>3</sub>	$M4$	$\pi^+, 0.85 \pm 0.3 / \pi^-, 1.7 \pm 0.25$
17.89	2 <sup>-</sup> + 4 <sup>-</sup>	0	(2 <sup>-</sup> ,0) <sub>13</sub> + (4 <sup>-</sup> ,0) <sub>6</sub>	$M2, E3 + E3, M4$	1.0±0.25
18.2				( $E3, M4$ )	
18.4				( $E3, M4$ )	
18.7	(3 <sup>-</sup> )	0 + 1		( $M2 + M4$ )	2.0±0.5(3 <sup>-</sup> ,0) <sub>12</sub>
20.1	(3 <sup>-</sup> )	0 + 1		( $M2 + M4$ )	2.0±0.5(3 <sup>-</sup> ,0) <sub>12</sub>

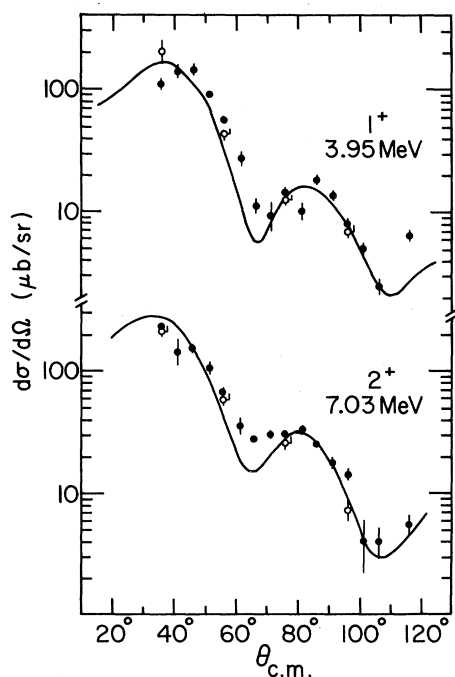


FIG. 3. Angular distributions for positive parity states. The solid points indicate  $\pi^+$  data, while the open points are  $\pi^-$  data. The curves are described in the text.

sition densities are described by harmonic oscillator wave functions, the value of the oscillator parameter being fixed to  $\langle r^2 \rangle = 7.036 \text{ fm}^2$ , a typical value used in calculating  $E2$  matrix elements in  $p$ -shell nuclei. The analysis of the elastic scattering discussed below uses a harmonic oscillator form for the matter density, the oscillator parameter being adjusted to provide the best overall agreement with the experimental data. As a result of these procedures, it should be noted that the oscillator parameters for the transition densities and for the matter density are not identical. This inconsistency is not of concern, however, since the matter density affects only the distorted waves and small changes in the input density distribution may correct deficiencies in the optical model. For weak transitions, however, significant deviations from the observed shapes may result from the use of a fixed scatterer reaction model. Recoil terms which are neglected in the current treatment can introduce additional components into the transition strength that may significantly alter both the shape and magnitude of differential cross sections.

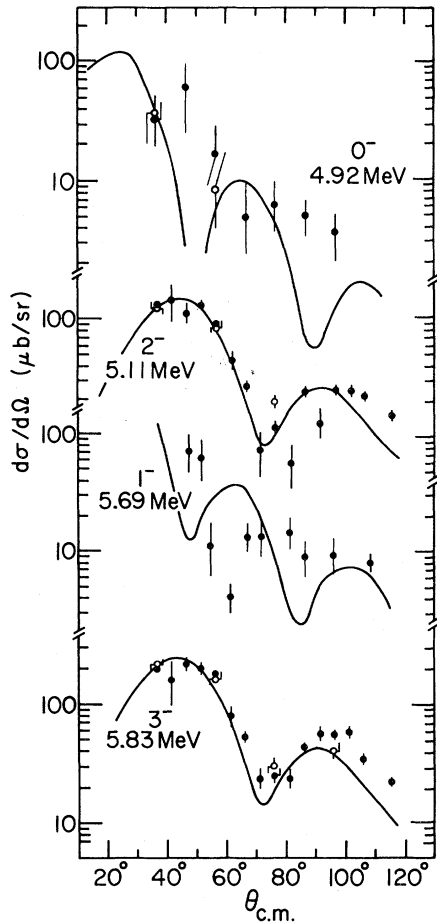


FIG. 4. Angular distributions for states of predominant configuration  $(2s,1d)^1(1p_{1/2})^{-1}$ . Solid points are  $\pi^+$  data while open points are  $\pi^-$  data. The curves are described in the text.

#### A. Elastic scattering

The elastic scattering data were fit by optical model calculations using two first order optical potentials. The importance of pion absorption makes it clear that first order potentials are not sufficient to describe all features of the scattering process, but they do provide a useful parametrization of the experimental data which should be adequate for the determination of the distorted wave functions required for the inelastic DWIA calculations. That such a procedure does give meaningful results has been demonstrated in several previous works. Two optical potentials which are widely used in the literature were employed: the coordinate space Kisslinger potential<sup>14</sup> and the first-order momentum space potential of Landau, Phatak, and Tabakin (LPT).<sup>15</sup> The elastic scattering calculations were

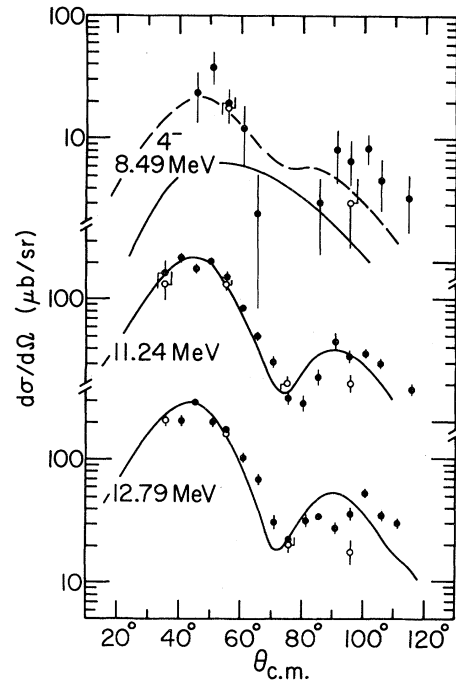


FIG. 5. Angular distribution for previously assigned negative parity states with excitation energies between 8 and 13 MeV. Solid points are  $\pi^+$  data while open points are  $\pi^-$  data. The curves are described in the text.

carried out with the computer codes FITPI (Ref. 16) (the Kisslinger potential) and PIPIT (the LPT potential).<sup>17</sup>

The Kisslinger potential was used to provide a simultaneous fit to the data for both  $\pi^+$  and  $\pi^-$  elastic scattering. Calculations using matter distributions obtained from analyses of electron scattering were not able to reproduce the cross sections in the region of the second maxima with variations of the complex strength parameters of the  $s$ - and  $p$ -wave interactions ( $b_0$  and  $b_1$ , respectively). An adequate fit could be obtained by adjusting the diffuseness of the matter distribution in addition to varying  $b_0$  and  $b_1$ . These calculations are shown as the dashed curves in Fig. 2; the fitted values of the optical model parameters are presented in the figure caption.

A harmonic oscillator density distribution was used in the PIPIT calculations. A grid search on the radius parameter found the best overall agreement with the data for an oscillator parameter  $b=1.7$  fm [ $\psi \sim \exp(-r^2/2b^2)$ ]. These results are shown as the solid curves in Fig. 2. This density distribution corresponds to a root mean square (rms) matter radius which is  $\sim 0.1$  fm larger than the experimental value determined in elastic electron scattering, in contrast

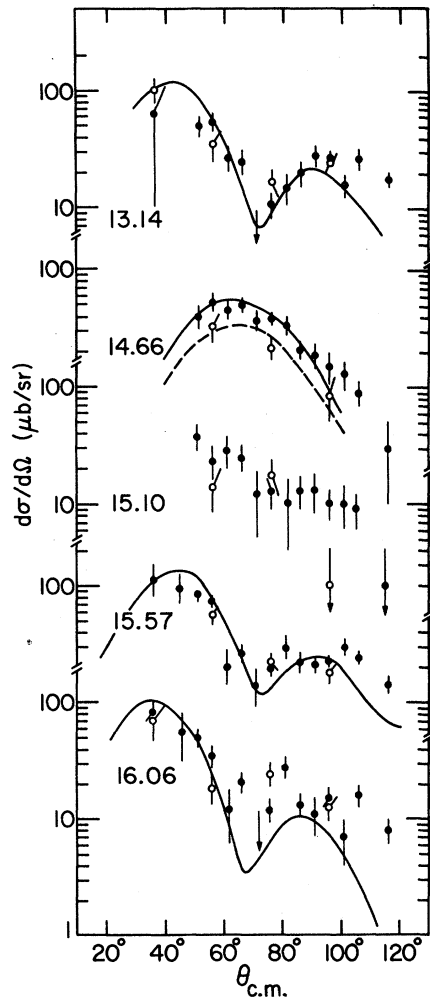


FIG. 6. Angular distributions for states at excitation energies between 13 and 16.5 MeV. Solid points indicate  $\pi^+$  data and open points indicate  $\pi^-$  data. The curves are described in the text. For the 14.66 MeV state, the dashed line is normalized to the  $\pi^-$  data.

to the situation in heavier nuclei where rms radii smaller than those inferred from the measured charge radii are required.<sup>18</sup> Since the DWIA calculations are formulated in momentum space, these last calculations provide the distorted waves used in the model for inelastic scattering.

The experimental elastic scattering cross sections are quite similar for  $\pi^+$  and  $\pi^-$ , as would be expected for scattering from a light  $T=0$  nucleus. As a consequence, the distorted wave functions are also similar, so that any differences between  $\pi^+$  and  $\pi^-$  cross sections for inelastic reactions must be due to isospin mixing in the nuclear structure, and not result from Coulomb effects in elastic scattering.

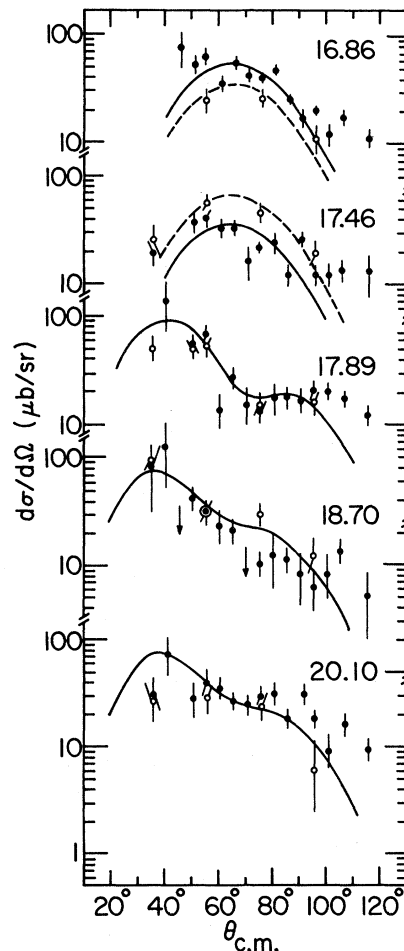


FIG. 7. Angular distributions for states above 16.5 MeV excitation. The curves are described in the text. Solid points are  $\pi^+$  data while open points are  $\pi^-$  data.

### B. Positive parity states

Only two positive parity states at 3.95 MeV ( $1^+$ ,  $T=0$ ) and 7.03 MeV ( $2^+$ ,  $T=0$ ) are strongly excited in  $\pi^+$  and  $\pi^-$  scattering on  $^{14}\text{N}$  (Fig. 1 and Table I). The 2.31-MeV ( $0^+$ ,  $T=1$ ) and 11.03 MeV ( $3^+$ ,  $T=0$ ) states are not observed. This result is consistent with the DWIA calculation of Lee and Kurath who find that only the  $1^+$  and  $2^+$  states have appreciable cross sections, the  $0^+$  and  $3^+$  states being reduced by at least an order of magnitude. No other strong positive parity transitions are predicted in the  $1p$  model space.

The calculated angular distributions for both  $\pi^+$  and  $\pi^-$  scattering to the 3.95 and 7.03 MeV levels are shown in Fig. 3. The DWIA optical parameters are those derived from fitting the elastic scattering and are similar to those used by Lee and Kurath

throughout the  $1p$  shell.<sup>2</sup> The theoretical shapes are essentially indistinguishable, being dominated by the  $E2$  amplitudes even though the  $M1$  amplitude for the  $2^+$  state is large. The shapes of the calculated angular distributions are in very good agreement with the experimental distributions, as is seen in Fig. 3. No difference is seen, nor is any predicted, between  $\pi^+$  and  $\pi^-$  scattering.

It has long been known that isoscalar  $E2$  transition amplitudes calculated with  $1p$  shell wave functions must be modified to obtain agreement with experimental results.<sup>19</sup> This is understood in terms of components of the wave function outside the  $1p$ -shell configuration space, namely those associated with the high-frequency giant quadrupole resonance. The effect of such configurations is assumed to modify the  $E2$  amplitudes within a given nucleus in a state independent fashion. Lee and Kurath<sup>2</sup> have shown that the same enhancement factors, i.e., factors multiplying the transition amplitudes, required to obtain agreement with  $E2$  gamma-decay rates in  $1p$ -shell nuclei yield reasonable agreement when used in analyses of inelastic pion scattering.

Comparisons of the data with theoretical predictions with no enhancement are presented in Table I. The normalization factors of  $1.45 \pm 0.2$  and  $2.2 \pm 0.3$  found for the 3.95-MeV state and the 7.03-MeV

state, respectively, correspond to  $E2$  enhancement factors of approximately 1.20 and 1.48 for these levels, and are somewhat lower than anticipated on the basis of scattering in nearby nuclei. With these enhancement factors, deduced values of  $B(E2)\uparrow$ , in units of  $e^2\text{fm}^4$ , are  $2.78 \pm 0.4$  for the  $1^+$  state at 3.95 MeV excitation and  $3.95 \pm 0.7$  for the  $2^+$  state at 7.03 MeV excitation. The larger enhancement for the  $2^+$  state may, in part, be due to the strong  $M1$  contribution known to connect this state to the ground state of  $^{14}\text{N}$ . Near the maximum of the angular distribution, however, the  $M1$  term is expected to provide only approximately 10% of the cross section; a sizable deviation from this prediction is required before a significant change in the  $E2$  enhancement is apparent.

A comparison of the present results with those in the literature is somewhat difficult because of the extreme variation in published values for transition probabilities,<sup>20</sup> as can be seen in Table II. The  $B(E2)\uparrow$  value for the  $1^+$  state is close to that obtained in electron scattering<sup>21</sup> and is in good agreement with a value of  $2.6 \pm 0.3$  obtained from a Doppler-shift-attenuation experiment.<sup>22</sup> All other measured values of  $B(E2)\uparrow$  for the  $1^+$  state are substantially larger. The ratio of transition probabilities for the  $1^+$  and  $2^+$  states is in good accord with

TABLE II. Reduced transition probabilities,  $B(\lambda)\uparrow$  in units of  $e^2\text{fm}^{2\lambda}$ . The predicted values involve no enhancement, i.e., bare nucleon charges. The references for previous values are presented in the column headings. When more than one value is shown, an additional source is referenced. The values for  $(\alpha, \alpha')$  were obtained from Ref. 7 by normalizing the average values of the matrix elements for the  $E3$  transitions to the 5.11- and 5.83-MeV levels to the present data. The values for the 13.13 MeV level assume a  $2^-$  assignment.

Level	$J^\pi$	Multipole	$B(\lambda)\uparrow$ ( $e^2\text{fm}^{2\lambda}$ )					
			Present	Predicted	$(e, e')^a$	$\gamma$ decay <sup>b</sup>	$(\alpha, \alpha')^c$	$(^3\text{He}, ^3\text{He})^d$
3.95	$1^+$	$E2$	$2.8 \pm 0.4$	1.93	$3.4 \pm 0.3$	$4.1 \pm 0.5$ $6.0 \pm 0.5^f$	$6.5^e$	6.5
7.02	$2^+$	$E2$	$3.95 \pm 0.7$	1.8		$6.0 \pm 1.5$ $3.6 \pm 1.2^f$	$5.5^e$	5.4
5.11	$2^-$	$E3$	$74 \pm 10$	64	$80 \pm 19$	$90 \pm 30$	77 $67^e$	70
5.83	$3^-$	$E3$	$117 \pm 18$	76	$166 \pm 35$		109 $140^e$	140
11.24	$3^-$	$E3$	$110 \pm 12$	58			123	
12.79	$4^-$	$E3$	$151 \pm 17$	84			155	
13.13	$(2^-)$	$E3$	$(31 \pm 8)$				(37)	
15.57	$2,3,4^-$	$E3$	$10(2J+1)$				$18(2J+1)$	

<sup>a</sup>Reference 21.

<sup>b</sup>Reference 1.

<sup>c</sup>Reference 7.

<sup>d</sup>Reference 24.

<sup>e</sup>Reference 23.

<sup>f</sup>Reference 20.

the latest compilation,<sup>1</sup> with each  $B(E2)\uparrow$  being about 30% low.

### C. Negative parity states

In contrast to the few  $(1p)^{-1}$  positive parity states predicted, the  $(2s,1d)^1(1p)^{-3}$  configuration gives rise to a very large number of states of negative parity, many of which are predicted to be strongly excited in inelastic pion scattering. Figure 8 shows the distribution in excitation energy of states in  $^{14}\text{N}$  whose calculated peak cross sections are greater than  $\sim 40 \mu\text{b}$ . In many cases both electric and magnetic transitions contribute to the excitation of states of a particular  $J$ , so that significant differences in the angular distributions are predicted for the same  $J$ . Weakly excited states ( $\leq 40 \mu\text{b}$ ) are not shown, since only slight changes in the phase and amplitude of the particle-hole admixtures can radically alter the shape and magnitude of the distributions.

The cross sections for the strong transitions of Fig. 8 were obtained from the approximation formulae presented in Ref. 2. For  $^{14}\text{N}$  which has a  $J=1$ ,  $T=0$  ground state, the estimated peak cross sections for exciting a  $J_i T_f$  final state are given by

$$\frac{d\sigma}{d\Omega}(\theta_{\text{peak}}, JLS) \simeq C_{JLS} \frac{(2J_f + 1)}{3} [16 - 12T_f] A_{JLS}^2.$$

Here  $A_{JLS}$  is the neutron transition density to the state  $J_f T_f$  and the constants for  $^{14}\text{N}$  are  $C_{431} = 4.7 \mu\text{b}$ ,  $C_{330} = 16.1 \mu\text{b}$ ,  $C_{211} = 12.2 \mu\text{b}$ , and  $C_{110} = 255 \mu\text{b}$ . For  $J=1$  and 2 both  $d$  and  $s$  amplitudes contribute,

$$A_{211} = A_{211d} + 0.56A_{211s},$$

$$A_{110} = A_{110d} + 0.56A_{110s}.$$

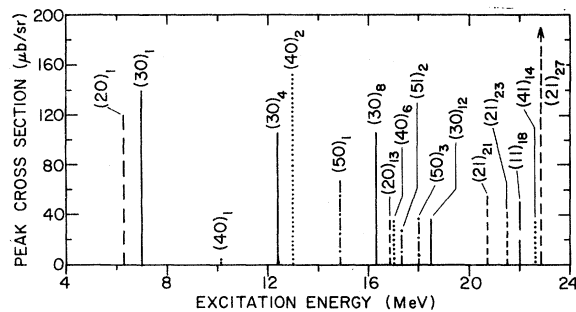


FIG. 8. Predicted excitation energies and peak cross sections for negative parity states in  $^{14}\text{N}$ . The lines indicate different spins and are self-explanatory. The notation  $(JT)_R$  indicates spin, isospin, and the number of the state, i.e.,  $(30)_8$  means the eighth  $3^-$  state. Only states predicted to have peak cross sections greater than  $40 \mu\text{b}$  are shown.

The calculated transition density amplitudes for transitions included in Fig. 8 are given in Table III, together with numerical values for the peak cross sections.

### 1. Valence configurations

The lowest negative parity states observed in  $\pi$  inelastic scattering by  $^{14}\text{N}$  are the doublets at 4.92 MeV ( $0^-$ ) and 5.11 MeV ( $2^-$ ) and at 5.69 MeV ( $1^-$ ) and 5.83 MeV ( $3^-$ ). Within each doublet it is the state with the higher spin value ( $2^-$  and  $3^-$ , respectively), which predominates. In a simple  $jj$  coupling model these two states would correspond to pure  $p_{1/2}d_{5/2}$  configurations. The validity of the description appears to be reflected in the relatively pure  $L=3$  calculated angular distributions shown in Fig. 4, which agree well with the experimental shapes. In contrast, the calculated  $L=1$  angular distributions for the  $0^-$  and  $1^-$  states (corresponding to a  $p_{1/2}s_{1/2}$  configuration) agree neither in shape nor magnitude with experiment, and, in addition, severely underpredict the already small experimental cross sections. While part of the disagreement may be due to the experimental difficulty of determining reliable cross sections for such weak states, the calculated angular distributions are also very sensitive to deviations from the model wave functions of these states. In view of the lack of agreement between the experiment and theoretical expectations, no information can be obtained for the  $0^-$  and  $1^-$  states. In electron scattering,<sup>21</sup> the transitions to these negative parity states are also quite weak and inconsistent with theoretical descriptions.

Comparison of the data to the predicted values yields an enhancement factor of 1.07 for the  $2^-$  state, while an enhancement factor of 1.24 is found for the  $3^-$  state. The corresponding reduced transition probabilities,  $B(E3)\uparrow$ , for the  $2^-$  and  $3^-$  states are listed in Table II. The agreement with previous results is excellent for the  $2^-$  state, where a consistent value of  $B(E3)\uparrow$  is obtained in both a variety of scattering experiments and the  $E3$  contribution to the radiative decay of the  $2^-$  state. For the  $3^-$  state, the current value for  $B(E3)\uparrow$  is somewhat smaller than is obtained from electron scattering, but is in agreement with that obtained from recent alpha particle scattering.<sup>7</sup> In summary, both the  $2^-$  and  $3^-$  states, as well as the positive parity states discussed in the preceding section, have angular distributions whose shapes are well described by the model. Except for the  $2^-$  state, the absolute magnitudes of the calculated cross sections, however, require enhancement to provide good agreement with the data. While the need for enhancement factors has been established previously for  $E2$  transitions,

TABLE III. Transition density amplitudes  $A_{JLSI}$  for neutrons to calculated negative parity states of  $^{14}\text{N}$ . The peak cross sections resulting from Eq. (1) are given in  $\mu\text{b}$  for each state. The numbers in parentheses ( $R$ ) indicate the  $R$ th state of a given  $J_f$  independent of  $T_f$ .

$J_f T_f R$	$J(LS)I$					
	4(31) $d$	3(30) $d$	2(11) $d$	2(11) $s$	1(10) $d$	1(10) $s$
00(1)					0.203	-0.533
$\sigma$					12	
10(1)			-0.040	0.052	0.183	-0.460
$\sigma$			0		23	
11(18)			0.137	0.044	0.176	0.073
$\sigma$			2		48	
20(1)		-0.522	0.159	-0.015	-0.013	0.029
$\sigma$		117	8		0	
20(13)		-0.164	0.225	0.254	0.015	-0.026
$\sigma$		12	43		0	
21(21)		-0.040	-0.134	-0.353	-0.136	-0.064
$\sigma$		0	9		50	
21(23)		0.236	-0.154	-0.094	0.115	0.070
$\sigma$		6	3		41	
21(27)		-0.015	-0.143	-0.015	0.462	0.116
$\sigma$		0	2		470	
30(1)	-0.032	0.481	-0.240	+0.023		
$\sigma$	0	139	24			
30(4)	0.129	0.421	-0.060	-0.002		
$\sigma$	3	106	2			
30(8)	-0.078	0.081	-0.301	-0.319		
$\sigma$	1	4	103			
30(12)	0.253	-0.035	-0.210	-0.096		
$\sigma$	11	1	32			
40(1)	0.145	-0.067				
$\sigma$	5	4				
40(2)	0.098	-0.444				
$\sigma$	2	152				
40(6)	-0.259	-0.213				
$\sigma$	15	35				
41(14)	-0.090	0.429				
$\sigma$	1	36				
50(1)	-0.500					
$\sigma$	69					
51(2)	0.649					
$\sigma$	29					
50(3)	-0.369					
$\sigma$	38					

there has been no unambiguous indication of a similar requirement for  $E3$  transitions in the  $1p$  shell.

## 2. States between 8- and 13-MeV excitation

At higher excitations in  $^{14}\text{N}$ , Fig. 8 shows that a  $3^-$  and a  $4^-$  state around 12–13 MeV are predicted to be strongly excited by essentially pure  $L=3$  transitions. Experimentally, two strong states are observed at 11.24 MeV and at 12.79 MeV whose angular distributions, shown in Fig. 5, exhibit charac-

teristic  $L=3$  shapes. Two negative parity states are known<sup>1</sup> at an excitation energy around 11.24 MeV, namely a state at 11.29 MeV with spin  $2^-$  and a state at 11.24 MeV with spin  $3^-$ . Both states would be excited by an  $L=3$  transition, but the model predicts that the strength is concentrated in the state with spin  $J=3^-$ . Around 12.79 MeV excitation only one negative parity state is tabulated, one at 12.82 MeV with spin  $4^-$ . Thus it seems reasonable to associate the 11.24- and 12.79-MeV states with the theoretically predicted  $3^-$  and  $4^-$  states. At the

same time the lowest  $4^-$  state at 8.49 MeV may be associated with the lowest theoretical  $4^-$  state at 10.0 MeV which has a predicted intensity too small to be seen in Fig. 8.

Calculated angular distributions for inelastic excitation of the 8.49 MeV ( $4^-$ ), 11.24 MeV ( $3^-$ ), and 12.79 MeV ( $4^-$ ) states are shown in Fig. 5. For the latter two states the agreement in shape is very good, although the intensity is again underpredicted by about a factor of 2, i.e., an enhancement factor of  $\sim 1.4$  in each case. For the 8.49 MeV ( $4^-$ ) state, the model predicts only a weak excitation of predominant  $M4$  shape (the solid curve in Fig. 5) which is in obvious disagreement with the experimental angular distribution. However, because the nearly  $4^-$  state at 12.79 MeV is strongly excited, even a small admixture with this state can introduce a significant  $E3$  amplitude into the 8.49 MeV wave function. A 4% admixture leads to the much improved agreement shown in Fig. 5 (the dashed line) without affecting the fit to the 12.79-MeV state.

It should also be noted that all three states have been previously observed in inelastic alpha<sup>23</sup> and  $^3\text{He}$  scattering<sup>24</sup> with approximately the same relative intensity as observed in the current study, but were not associated with specific states in  $^{14}\text{N}$ . Recently, higher resolution alpha scattering<sup>7</sup> has been performed which agrees with the present excitation energies, identifications, and transition strength.

### 3. Excitation energies above 13 MeV

The energies of the peaks observed above 13 MeV excitation are listed in Table I although, because of the rapid increase in  $^{14}\text{N}$  level density with increasing excitation energy, it is not possible to directly associate an observed peak with a particular state in  $^{14}\text{N}$ . The angular distributions for some of these peaks are shown in Figs. 6 and 7 and, in the following, an attempt will be made to relate the observed peaks with the states predicted to be excited strongly.

**13.14 MeV.** The peak at 13.14 MeV listed in Table I lies on the upper edge of the strongly excited 12.79 MeV state. Despite the incomplete separation, an angular distribution for this state has been extracted which exhibits a characteristic  $L=3$  shape. A known  $2^-$  state at 13.24 MeV excitation could correspond to such a transition, but no  $2^-$  state is predicted (Fig. 8) to be strongly excited in this region of excitation. An  $L=3$  transition is also observed at  $E_{\text{ex}}=13.13$  MeV in alpha scattering<sup>7</sup> with approximately the same relative strength.

**14.66 MeV.** The angular distribution of this state is much flatter than the characteristic  $L \leq 3$  shapes observed for states at lower excitation energies. The

excitation energy agrees well with the theoretical  $5^-$  state predicted at 14.84 MeV. The calculated angular distribution for inelastic pion scattering to this level is shown in Fig. 6 and reproduces both the shape and approximate magnitude of the experimental distribution. We therefore identify the 14.66 MeV peak as the first  $5^-$  level in  $^{14}\text{N}$ . The tabulation<sup>1</sup> lists a  $2^-$  state at 14.66 MeV but this cannot correspond to the state observed in the present experiment. There are several other levels in the vicinity with unattributed spins.

The relatively strong excitation of this  $5^-$  state is associated with the particle-hole stretched configuration  $[(p_{3/2})^{-1}d_{5/2}]_{4-}$  coupled to the  $1^+$  of the  $^{14}\text{N}$  ground state. The prominence of the  $4^-$  stretched configuration in pion inelastic scattering has already been observed with  $^{12}\text{C}$ ,  $^{13}\text{C}$ , and  $^{16}\text{O}$  targets.<sup>5,6,25</sup> The data shown in Fig. 6 seem to show a difference between the  $\pi^+$  and  $\pi^-$  cross sections, although the statistical errors preclude a definitive evaluation of the magnitude.

**15.1 MeV.** The peak at 15.1 MeV listed in Table I is weakly excited in inelastic pion scattering and only an incomplete angular distribution could be obtained. It could not be fitted but appears to have a shape characteristic of  $L > 3$ .

**15.6 and 16.1 MeV.** The experimental angular distributions of the 15.6 MeV state and of the 16.1 MeV state are shown in Fig. 7. They appear very similar with shapes characteristic of  $L=3$ . An  $L=3$  transition is also observed in inelastic alpha scattering<sup>7</sup> at  $E_x=15.4$  MeV, so that an  $E3$  excitation is indicated for the 15.6 level. A  $3^-$  state which is strongly excited by a predominantly  $M2$  transition is predicted at 16.26 MeV. The calculated  $M2$  angular distribution is compared to the 16.1 MeV state in Fig. 6. Its shape is very similar to that for an  $E3$  transition except that the first maximum occurs a few degrees more forward in angle. Although the agreement with experiment is reasonable, the data do not extend far enough forward nor are they of sufficiently good quality to permit an unambiguous  $M2$  determination. However, in support of the current assignment, it should be noted that recent inelastic electron scattering<sup>8</sup> on  $^{14}\text{N}$  finds a transition to a 16.11 MeV state which exhibits  $M2$  strength. The absence of the peak in inelastic alpha scattering is also consistent with this interpretation.

**16.86 and 17.46 MeV.** The angular distributions for  $\pi^+$  and  $\pi^-$  inelastic scattering to these states are shown in Fig. 7. Both angular distributions appear characteristic of  $L > 3$  transitions. In addition, however, the excitation of these states appears to exhibit significant differences between  $\pi^+$  and  $\pi^-$  scattering, the  $\pi^-$  scattering being weaker for the 16.86

MeV state and stronger for the 17.46 MeV state. Separate normalizations for the calculated angular distributions are shown as the solid and dashed curves for  $\pi^+$  and  $\pi^-$ , respectively. As shown in Fig. 8, two  $5^-$  states are predicted in this region, at 17.31 MeV ( $T=1$ ) and at 18.00 MeV ( $T=0$ ), both of which are expected to be excited by pure  $M4$  with reasonable strength. Unfortunately the fit to the experimental distributions with a pure  $M4$  shape is only marginal, in each case the  $\pi^+$  data points being flat over a wider region than predicted. Paradoxically, the more limited  $\pi^-$  angular distributions appear to be better fitted. Nevertheless, despite the limited agreement, it is tempting to associate these states with the two  $5^-$  states predicted theoretically and, in view of the complementary  $\pi^+/\pi^-$  ratios, to invoke isospin mixing. The compilations indicate a  $5^-$  state at 16.91 MeV which is isospin mixed, but no state in  $^{14}\text{N}$  is listed in the vicinity of 17.5 MeV excitation. The summed strength of those levels together with that of the 14.66 MeV state nearly exhaust the total  $5^-$  strength predicted for  $^{14}\text{N}$ . This is in contrast to data for other  $1p$ -shell nuclei where a substantial fraction of the strength for stretched configurations is not identified.

*17.9 MeV.* The angular distribution of this peak is shown in Fig. 7. Only limited data of poor statistics could be obtained at forward angles because the hydrogen elastic peak occurs in this region of the melamine spectrum. As shown in Fig. 8, the theory predicts a  $2^-$  and a  $4^-$  close-lying doublet to be relatively strongly excited in this region of excitation. While the calculated distribution for the  $2^-$  state (not shown) reproduces the observed shape reasonably well, the sum of the angular distribution predicted for each state gives very good agreement in both shape and magnitude. No guidance is provided by the compilation since no states are listed at this excitation energy.

*18.2 and 18.4 MeV.* An apparent doublet at these energies is weakly excited in both  $\pi^+$  and  $\pi^-$  inelastic scattering. Because of the low intensity and uncertainty in the choice of background level, a reliable angular distribution could not be obtained over the full range of angles studied, although the data appear to exclude  $L < 3$ . Two  $3^-$  states, at 18.2- and 18.4-MeV excitation, are listed in the compilation.

*18.7 MeV.* The experimental angular distribution is shown in Fig. 7 and it appears typical of an  $L \geq 3$  distribution. The theory predicts a  $3^-$  state at 18.5 MeV which should be excited primarily by  $M2 + M4$  transitions. The calculated angular distribution compares well with the data in shape, although the magnitude is underestimated by about a factor of 2. No state is tabulated at this excitation energy.

*20.1 MeV.* A peak at this energy is observed in both  $\pi^+$  and  $\pi^-$  with reasonable intensity. Its angular distribution is characteristic of  $L \geq 3$  and, although flatter than that of the 18.7 MeV state shown in Fig. 7, it can be reasonably fitted by the calculated 18.5 MeV ( $3^-$ ) distribution. The only other high-spin state predicted theoretically in this region is the  $4^-$ ,  $T=1$  state at 22.63 MeV (Fig. 8), but the predicted pure  $E3$  transition would give a more strongly forward-peaked angular distribution. Only a  $1^-$ ;  $T=0 + 1$  state at 20.1 MeV excitation is listed in this energy region. As is seen in Fig. 1, carbon contributions are large in this vicinity.

Before concluding the discussion of the states excited at high excitation energy in  $^{14}\text{N}$ , two general problems may be noted. In the first place, Fig. 8 shows that several  $2^-$  and  $1^-$  states, including the giant  $E1$  resonance, are predicted to be strongly excited above  $E_x \approx 20$  MeV in pion inelastic scattering. Although data at angles more forward than those covered in the current study are required to firmly establish the location of these states, it is surprising that no groups beyond  $E_x \approx 20$  MeV appear to be excited in, for example, the  $35^\circ$  spectra. Of course, the subtraction procedure ( $\text{CH}_2\text{N}_2\text{-CH}_2$ ) which generates the  $^{14}\text{N}$  spectrum results in the greatest background problems at forward angles.

In the second place, the experimental angular distributions for the highly excited states appear consistently flatter than the theoretical distributions. This may be a problem of the choice of background used in the peak-fitting program, particularly in cases where peaks are incompletely resolved. Clearly, use of an elemental  $^{14}\text{N}$  target and better counting statistics in the region of high excitation energies could improve the quality of the data.

#### 4. Isospin mixing

Differences in the cross sections for  $\pi^+$  and  $\pi^-$  scattering to the states at 14.66-, 16.9-, and 17.5-MeV excitation have already been noted. While apparent differences are also observed in the relative intensities of  $\pi^+$  and  $\pi^-$  scattering to other peaks in the spectra at particular angles, the evidence is inconclusive, as can be seen from the angular distributions shown in Figs. 6 and 7. Apart from the differences observed in the peaks around 17 MeV, deviations from equality in other cases are not outside the statistical uncertainty of the data. Calculations utilizing a residual interaction to generate isospin mixing have also been performed. These calculations indicate that significant differences between  $\pi^+$  and  $\pi^-$  scattering are expected only for  $5^-$  states. With an off diagonal matrix element of  $\sim 100$  keV, the predicted cross section ratios,  $\pi^+$  to  $\pi^-$  scattering, are 1.27, 1.5, and 0.65 for  $(5^-,0)_1$ ,  $(5^-,1)_2$ , and

$(5^-, 0)_3$ , respectively. A calculation explicitly including the Coulomb interaction gives similar results. In view of the large uncertainties, the agreement between these values and those shown in Table I is quite satisfactory.

### V. CONCLUSION

Pion scattering by  $^{14}\text{N}$  has been studied at  $T_\pi = 162$  MeV. The data have been analyzed within a model which incorporates shell model wave functions into a distorted wave impulse approximation formulated in momentum space. The analysis of the data for the low lying states, which have been studied extensively by other means, indicates that the model provides reasonable predictions for both the shapes and magnitudes of angular distributions. In view of the diversity of values in the literature, the need for enhancement in  $E3$  transitions in  $^{14}\text{N}$  has not been established. Except for the transition to the  $2^-$  state at 5.11-MeV excitation, however, there does appear a need for enhancement in the  $E3$  transitions observed in the current study.

For higher-lying negative parity states, there is also good agreement between the model and experimental data, both present and previous. This supports the tentative spin-parity assignments and provides possible shell model descriptions of the wave functions for these states, although state-dependent

renormalizations are required to fit absolute cross sections. Above 13 MeV excitation, where the density of states precludes a definitive correspondence between the present data and tabulated energy levels, the use of the model permits tentative assignment of several new levels and a description of their structure. In particular, the data suggest that the yrast  $5^-$  state lies at 14.66 MeV excitation and that it is excited by an  $M4$  transition of the form  $(d_{5/2}^1 p_{3/2}^{-1})_{4^-}$ . Other  $5^-$  states are also proposed and there is evidence for isospin mixing between a  $T=0, 1$  pair at approximately 17 MeV excitation.

In conclusion, it is seen that in a comparatively complicated nucleus such as  $^{14}\text{N}$ ,  $\pi^\pm$  scattering analyzed with a suitable model for both structure and reaction mechanism can not only provide agreement with information derived in other ways, but also provide new nuclear structure information, particularly for highly excited states. At the same time, the present study provides a guideline for future work, since the validation of the structure calculations suggests further experiments with other probes. The availability of detailed theoretical predictions for  $^{14}\text{N}$  makes for a sensitive test of both experiment and theory.

This research was supported by the U.S. Department of Energy under Contract W-31-109-Eng-38 and by the National Science Foundation.

\*Permanent address: University of Birmingham, Birmingham, England.

† Present address: Indiana University, Bloomington, IN 47401.

‡ Present address: University of North Carolina, Chapel Hill, NC 27514.

§ Present address: University of South Carolina, Columbia, SC 29201.

<sup>1</sup>F. Ajzenberg-Selove, Nucl. Phys. **A360**, 1 (1981).

<sup>2</sup>T. S. H. Lee and D. Kurath, Phys. Rev. C **21**, 293 (1980); **21**, 1670 (1980).

<sup>3</sup>S. Cohen and D. Kurath, Nucl. Phys. **73**, 1 (1965).

<sup>4</sup>D. J. Millener and D. Kurath, Nucl. Phys. **A255**, 315 (1975).

<sup>5</sup>C. L. Morris *et al.*, Phys. Lett. **86B**, 31 (1970).

<sup>6</sup>D. B. Holtkamp *et al.*, Phys. Rev. Lett. **45**, 420 (1980).

<sup>7</sup>R. J. Peterson and J. J. Hamill, Z. Phys. A **305**, 275 (1982).

<sup>8</sup>N. Ensslin, L. W. Fagg, R. A. Lindgren, W. L. Bendel, and E. C. Jones, Phys. Rev. C **19**, 569 (1979).

<sup>9</sup>H. V. Smith, Phys. Rev. C **6**, 441 (1972).

<sup>10</sup>H. A. Thiessen *et al.*, Los Alamos Scientific Laboratory Report LA-4534-MS, 1970 (unpublished).

<sup>11</sup>J. R. Comfort, Argonne National Laboratory Physics

Division Informal Report PHY-1970B, 1970 (unpublished).

<sup>12</sup>K. Boyer *et al.* (unpublished).

<sup>13</sup>P. J. Bussey *et al.*, Nucl. Phys. **B58**, 363 (1973).

<sup>14</sup>L. S. Kisslinger, Phys. Rev. **98**, 761 (1955).

<sup>15</sup>R. Landau, S. Phatak, and F. Tabakin, Ann. Phys. (N.Y.) **78**, 299 (1973).

<sup>16</sup>M. D. Cooper and R. A. Eisenstein, Los Alamos National Laboratory Report No. LA6929 MS, 1971 (unpublished).

<sup>17</sup>R. A. Eisenstein and F. Tabakin, Comput. Phys. Commun. **12**, 237 (1976).

<sup>18</sup>C. Olmer *et al.*, Phys. Rev. C **21**, 254 (1980).

<sup>19</sup>D. Kurath, Nucl. Phys. **14**, 398 (1960).

<sup>20</sup>A. Ajzenberg-Selove, Nucl. Phys. **A268**, 1 (1976).

<sup>21</sup>N. Ensslin *et al.*, Phys. Rev. C **9**, 1705 (1974).

<sup>22</sup>M. Bister, A. Anttila, M. Piiparinen, and M. Viitasalo, Phys. Rev. C **3**, 1972 (1971).

<sup>23</sup>B. G. Harvey, J. R. Meriwether, J. Mahoney, A. Busiere de Nercy, and D. J. Horen, Phys. Rev. **146**, 712 (1966).

<sup>24</sup>G. C. Ball and J. Cerny, Phys. Rev. **177**, 1466 (1969).

<sup>25</sup>S. J. Seestrom-Morris, D. Denhard, D. B. Holtkamp, and C. L. Morris, Phys. Rev. Lett. **46**, 1447 (1981).